ORIGINAL ARTICLE

High strain rate response of CP-titanium under low-temperature conditions: experiment and modeling

Mateusz Kopec[1,3] · **Magdalena Łazińska**[2] · **Jacek Janiszewski**[2]

Received: 4 June 2025 / Revised: 9 July 2025 / Accepted: 24 August 2025

Abstract
This study investigates the dynamic mechanical behavior and microstructural evolution of commercially pure titanium (CP-Ti) under high-strain-rate loading at subzero temperature. Using a Split Hopkinson Pressure Bar setup equipped with a cryogenic environmental chamber, CP-Ti specimens were dynamically compressed at − 100 °C across strain rates of 1×10^3 s^{-1} and 2×10^3 s^{-1}. The results show a significant increase in flow stress at − 100 °C compared to room temperature, with peak true stresses reaching approximately 825 MPa at 2×10^3 s^{-1} and 730 MPa at 1×10^3 s^{-1} representing ~ 25–30% higher values than those observed at 22 °C. Electron backscatter diffraction analysis revealed a transition in deformation mechanisms with increasing strain rate and decreasing temperature. At room temperature, plastic deformation was predominantly accommodated by dislocation slip and deformation twinning. At low temperature, while twinning activity intensified, it was eventually superseded by shear band formation, indicating the onset of strain localization. A physically based viscoplastic constitutive model incorporating dislocation density evolution and thermally activated mechanisms was developed and calibrated against experimental data. The model accurately captured the stress–strain behavior across all tested conditions, with deviations below 5%, demonstrating its suitability for predictive simulations of low-temperature forming processes in HCP metals.

Keywords CP-Ti · Split Hopkinson Pressure Bar · Low temperature · Deformation twinning · Shear bands · Constitutive modeling

1 Introduction

Titanium alloys are widely utilized in high-performance industries such as aerospace, automotive, and biomedical sectors due to their exceptional strength-to-weight ratio, corrosion resistance, and high-temperature stability [1, 2]. However, their limited formability at room temperature presents a major challenge in manufacturing processes [3]. Unlike aluminum or steel alloys, which can be readily formed at ambient conditions, titanium alloys exhibit poor ductility and high flow stress at low and moderate temperatures, often requiring elevated temperatures to facilitate deformation [4]. This constraint significantly impacts industrial forming efficiency, energy consumption, and overall production costs. One of the promising solutions to overcome these limitations is Fast Alloy Stamping Technology (FAST), an advanced thermomechanical processing technique designed to enhance the formability of lightweight alloys by optimizing strain rate and temperature conditions [5]. Extending the forming window of

Published online: 29 August 2025

titanium alloys to lower temperatures while maintaining desirable mechanical properties is crucial for advancing industrial-scale applications [6].

Despite extensive research on the high-temperature deformation of titanium alloys, relatively little attention has been given to their mechanical behavior and microstructural evolution under high-strain-rate loading at subzero temperature. Understanding how titanium alloys respond to rapid deformation at low temperatures is critical for optimizing industrial forming processes and developing materials with superior mechanical performance. In particular, high-strain-rate deformation in the subzero regime can lead to unique strengthening mechanisms, including strain hardening, deformation twinning, and stress-induced phase transformations, which can significantly influence material behavior. The study [7] investigates the impact toughness and deformation mechanisms of the near-α titanium alloy CT20 at temperatures ranging from 20 to − 196 °C. The results show that impact toughness remains relatively high down to − 100 °C but decreases significantly at − 196 °C, where brittle fracture occurs. Crack propagation becomes less tortuous with decreasing temperature, as cracks cut through α lamellae rather than being deflected at grain boundaries. At higher temperatures, deformation is characterized by severe plasticity, lamellar α kinking, and extensive deformation twinning. As temperature decreases, twin density increases near the crack path, but fewer twins and lower geometrically necessary dislocation (GND) densities are observed in regions farther from the fracture surface, indicating reduced plasticity. The combination of crack path tortuosity, dislocation slip, and deformation twinning enhances impact toughness at 20 °C, while at − 196 °C, reduced plastic deformation capacity leads to brittle fracture with a small plastic zone. Another study [8] examines the impact behavior of Ti6Al4V alloy at 298 K, 223 K, and 77 K, revealing a decrease in impact toughness with temperature reduction. The toughness drops from 53.3 J/cm^2 at 298 K to 21.2 J/cm^2 at 77 K, with a shift in energy distribution favoring crack initiation over propagation at lower temperatures. Microstructural analysis shows that {1012}α twins form under impact at 298 K and 223 K but are absent at 77 K, indicating that twinning enhances toughness at higher temperatures. At 77 K, reduced plasticity, a straighter crack path, and minimal twin formation lead to brittle fracture. The findings highlight the role of twinning and dislocation slip in maintaining toughness and provide insights for optimizing Ti6Al4V alloy for low-temperature applications.

A key experimental approach for studying the dynamic response of materials is the Split Hopkinson Pressure Bar (SHPB) technique, which allows for precise characterization of high-strain-rate deformation in a controlled environment [9]. SHPB testing at low temperatures provides critical data on how strain rate sensitivity, adiabatic heating, and thermal softening affect the stress–strain response of titanium alloys [10]. In addition, microstructural changes such as grain refinement, dynamic recrystallization, and twin formation can be investigated through electron backscatter diffraction (EBSD) offering insights into the underlying deformation mechanisms [11]. These findings are essential for optimizing forming techniques such as FAST, where precise control over strain rate and temperature is necessary to achieve enhanced formability without compromising mechanical integrity.

To accurately describe the deformation behavior of titanium alloys at low temperatures, advanced mechanism-based viscoplastic constitutive models are required [9, 10]. Traditional empirical models often fail to capture the complex interplay between strain rate sensitivity, thermal activation, and microstructural evolution. In contrast, physically based constitutive equations incorporate fundamental deformation mechanisms, such as dislocation motion and phase transformations, enabling more accurate predictions of material response under dynamic loading [12]. Jeon et al. [12] proposed an elasto-visco-plastic self-consistent polycrystal model to represent the temperature-dependent plastic deformation behavior of CP-Ti. The model successfully reproduced various experimental behaviors, including stress vs. strain curves, diffraction lattice strains, twin volume fraction, and crystallographic texture. The development and validation of such models using experimental data are crucial for improving finite element simulations of industrial forming processes and optimizing process parameters for large-scale manufacturing.

This study aims to systematically investigate the mechanical response and microstructural evolution of titanium alloys subjected to SHPB testing at a temperature of − 100 °C. By integrating experimental results with mechanism-based constitutive modeling, the work aims to enhance the understanding of how CP-Ti behaves under extreme conditions and explore new possibilities for expanding their forming window in industrial applications.

The findings will contribute to the advancement of FAST and other high-strain-rate forming techniques, ultimately leading to more efficient and cost-effective manufacturing of titanium components with superior mechanical properties.

2 Materials and methods

2.1 Microstructural characteristics of the as-received CP-Ti

The microstructure of the as-received, commercial CP-Ti tested in this research is presented in Fig. 1 in the form of an Inverse Pole Figure (IPF) maps. The undeformed material exhibits equiaxed grains with preferred grain orientation of [0001].

2.2 2.2 Mechanical testing

Dynamic testing was carried out using the SHPB stand equipped with low-temperature environmental chamber. It is the most used technique for material testing at high strain rates [21]. Typical SHPB consists of a striker bar, input, and output bars, between which a cylindrical specimen is placed, Fig. 2. All bars of the SHPB device are made of the maraging steel (heat-treated MS350 grade: yield strength—2300 MPa; elastic wave speed—4960 m/s) with diameter of 12 mm. The lengths of the striker bar and input bar, as well as the output bar, were 250 and 1200 mm, respectively. The striker bar is driven by a gas gun with a barrel length of 1200 mm and inner diameter of 12.1 mm. To minimize the wave dispersion and to facilitate stress equilibrium, the pulse shapers were used. They had a shape of a disc made of copper and were placed on the impact end of the input bar. Trial tests were conducted to find the appropriate size of the pulse shaper. It was found that for a given SHPB test condition (i.e., mainly for given level of striker bar impact velocity), the copper pulse shaper with the diameter of 3 mm and thickness of 0.1 or 0.2 mm ensures damping of the high-frequency oscillations. Dynamic compression curves were plotted using the well-known formulas according to the classical Kolsky theory based on the single-wave analysis method, which assumes stress equilibrium for specimen under given testing conditions. The strain and strain rate in the specimens were calculated applying the reflected wave profile (ε_r), whereas the plastic flow stress in the specimen was determined from transmitted wave profile (ε_t). Wave signals were measured by pairs of strain gages (gage length—1.5 mm; resistance—350 Ohm) located at the half-length of the input and output bars (Fig. 2). The signals from the strain gages were conditioned by the data-acquisition system including a Wheatstone

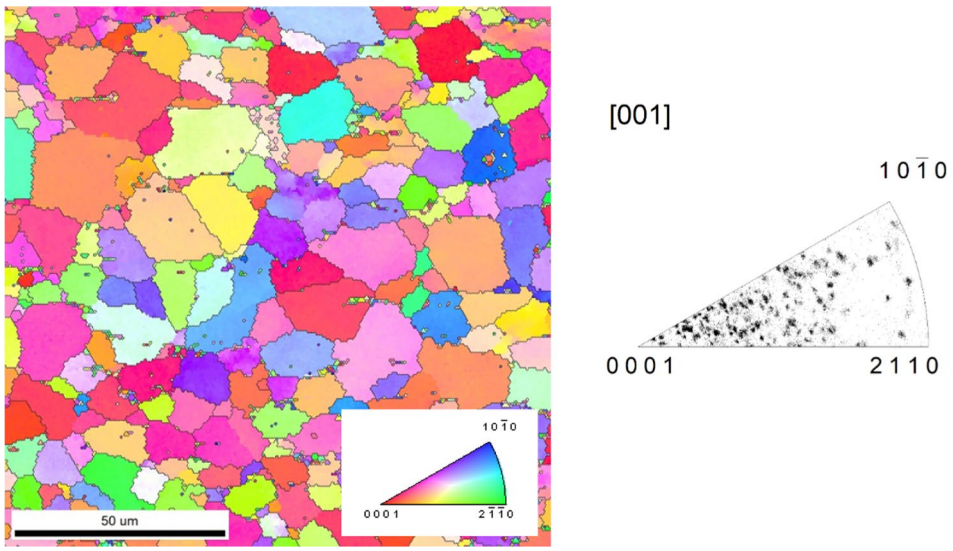

Fig. 1 IPF map of the as-received CP-Ti

 https://doi.org/10.1007/s43452-025-01317-0

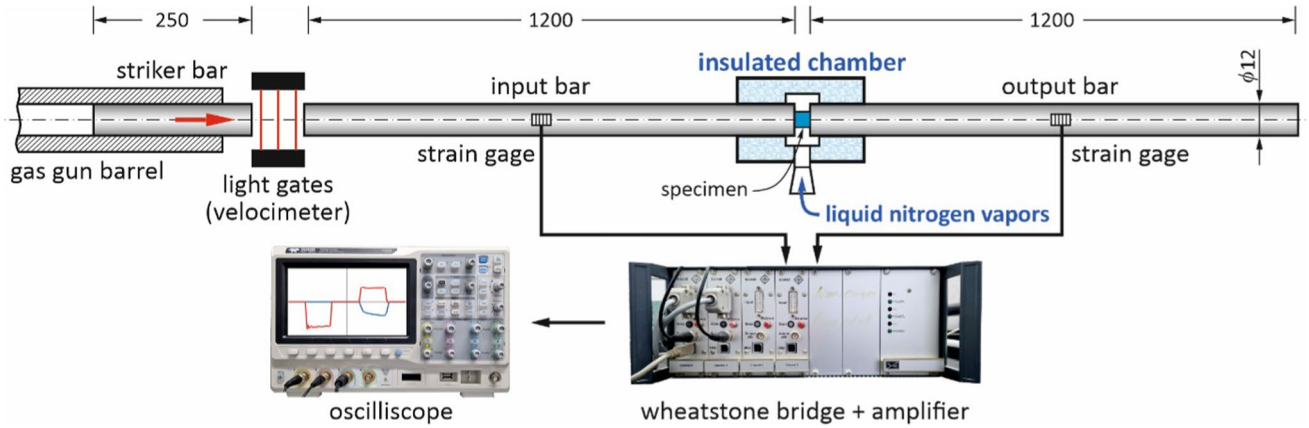

Fig. 2 Scheme of the SHPB system equipped with the environmental chamber for low-temperature testing

bridge, signal amplifier of the cut-off frequency equal to 1 MHz and digital oscilloscope. The dynamic tests at low temperature were conducted in the insulated chamber inside which the specimens machined from the extruded bar to cylindrical specimens of 5 mm × 5 mm were cooled down using liquid nitrogen. The chamber made of high-density polystyrene foam was divided into two parts, upper and lower, to facilitate its assembly on the Hopkinson bars and the placement of specimen between the bars. The chamber was equipped with a window through which the liquid nitrogen vapors were introduced. A thermocouple feedback processing controller was used to control the flow liquid nitrogen vapors using the cryogenic electrovalve. The thermocouple was in contact with the specimen from its upper side, i.e., on the side opposite to the specimen surface, which was cooled with liquid nitrogen vapors. In this way, the amount of liquid nitrogen vapors introduced into the chamber was controlled to keep a constant temperature for a long time. Based on the preliminary tests with reference specimen (specimen with a small hole in which the thermocouple was placed in the center of the longitudinal specimen axis), it was found out that after reaching the desired level, the temperature was held constant for at least 5 min to ensure no temperature gradient throughout the specimen. The mechanical property of the CP-titanium was characterized at strain rates ranging from 1×10^3 1/s to 2×10^3 1/s and a temperature of − 100 °C. The additional tests under the same conditions, however, at room temperature were performed for the comparative studies.

2.3 Microstructural observations

The microstructure of deformed specimens was characterized by SEM. Prior to the study, the specimens were first cold-mounted, and then polished using Struers MD-Largo disc dedicated to soft materials of 40-150HV and 9 µm diamond suspension. The polishing was performed using Metrep® MD-Chem cloth and 0.04 µm Colloidal Silica solution. The microstructural characterization was performed on high-resolution Quanta 3D FEG (SEM/FIB) scanning electron microscope system equipped with an integrated EDS/EBSD system (EDS—energy dispersive X-ray detector, and EBSD—electron backscatter diffraction analysis system) operated at 20 kV. The average grain size was calculated using NIS Elements software on the image magnification of 500×.

3 Results and discussion

3.1 Mechanical testing

The true stress–strain curves presented in the figure illustrate the dynamic mechanical response of commercially pure titanium (CP-Ti) subjected to high-strain-rate loading at two different temperatures, 22 °C (room temperature—green curves) and − 100 °C (blue curves), and two strain rates, 1×10^3 s^{-1} and 2×10^3 s^{-1} (Fig. 3). The

figure clearly demonstrates that CP-Ti exhibits significant strain rate sensitivity, as the flow stress increases with increasing strain rate. At both temperatures, the curves corresponding to the higher strain rate (2×10^3 s^{-1}) show higher peak stresses than those at the lower strain rate (1×10^3 s^{-1}). This behavior is characteristic of titanium and other hexagonal close-packed (HCP) metals, where deformation mechanisms such as dislocation motion and twinning are strongly influenced by strain rate [13]. Higher strain rates reduce the time available for thermal relaxation processes, leading to increased dislocation accumulation and work hardening, thereby raising the overall flow stress of the material [14]. A comparison of the stress–strain curves at 22 °C and − 100 °C reveals that CP-Ti exhibits higher flow stresses at lower temperatures for both strain rates. This temperature-dependent strengthening effect is a result of reduced dislocation mobility and thermal activation at subzero temperatures [15]. At lower temperatures, dislocations face greater resistance to movement, leading to higher stress levels required to sustain plastic deformation [9]. Furthermore, the suppression of dynamic recovery mechanisms, such as cross-slip and climb, contributes to increased strain hardening at − 100 °C. The initial stress–strain curves shows a steep rise in stress, indicating the elastic and early plastic deformation stages. As plastic deformation progresses, strain hardening becomes prominent, particularly at − 100 °C, where the material exhibits a more pronounced hardening rate before reaching peak stress. At room temperature, CP-Ti primarily deforms through dislocation slip, while at − 100 °C, deformation twinning is likely activated as an additional deformation mode due to the limited mobility of dislocations at low temperatures [16]. The activation of twinning can enhance strain hardening, contributing to the observed increase in flow stress and altering the material's plasticity [17–19].

3.2 Microstructural observations

The EBSD IPF maps presented in Fig. 4 illustrate the microstructural evolution of commercially pure titanium subjected to dynamic compression at varying strain rates and temperatures. At a moderate strain rate of $\dot{\varepsilon} = 1\times10^3$ s^{-1} and room temperature (Fig. 4a), the microstructure retains a predominantly equiaxed grain structure with limited evidence of severe distortion. Numerous well-defined deformation twins (yellow arrows) are visible within grains. These twins exhibit a sharp contrast in IPF orientation maps and span significant portions of grains, indicating that twinning plays a primary role in accommodating plastic strain under these conditions. The preservation of grain morphology and relatively homogeneous orientation distribution suggests that dislocation slip and twinning act synergistically to distribute strain without substantial strain localization. In contrast, the corresponding condition at − 100 °C (Fig. 4b) reveals a markedly different microstructural response. Although twinning activity is still prevalent—evident from the presence of thick and intersecting twin bundles—the microstructure exhibits signs of increasing orientation fragmentation and intragranular misorientation. This is seen as more complex and irregular IPF color patterns within grains, indicating significant crystallographic reorientation. At the subzero temperature, dislocation mobility is reduced, which favors the activation of deformation twinning as a compensatory mechanism. However, the higher resistance to dislocation slip also promotes the early

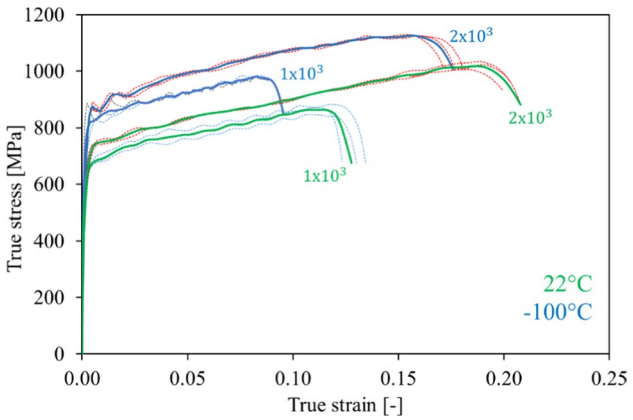

Fig. 3 Dynamic response of CP-Ti compressed under different values of strain rate and temperature

https://doi.org/10.1007/s43452-025-01317-0

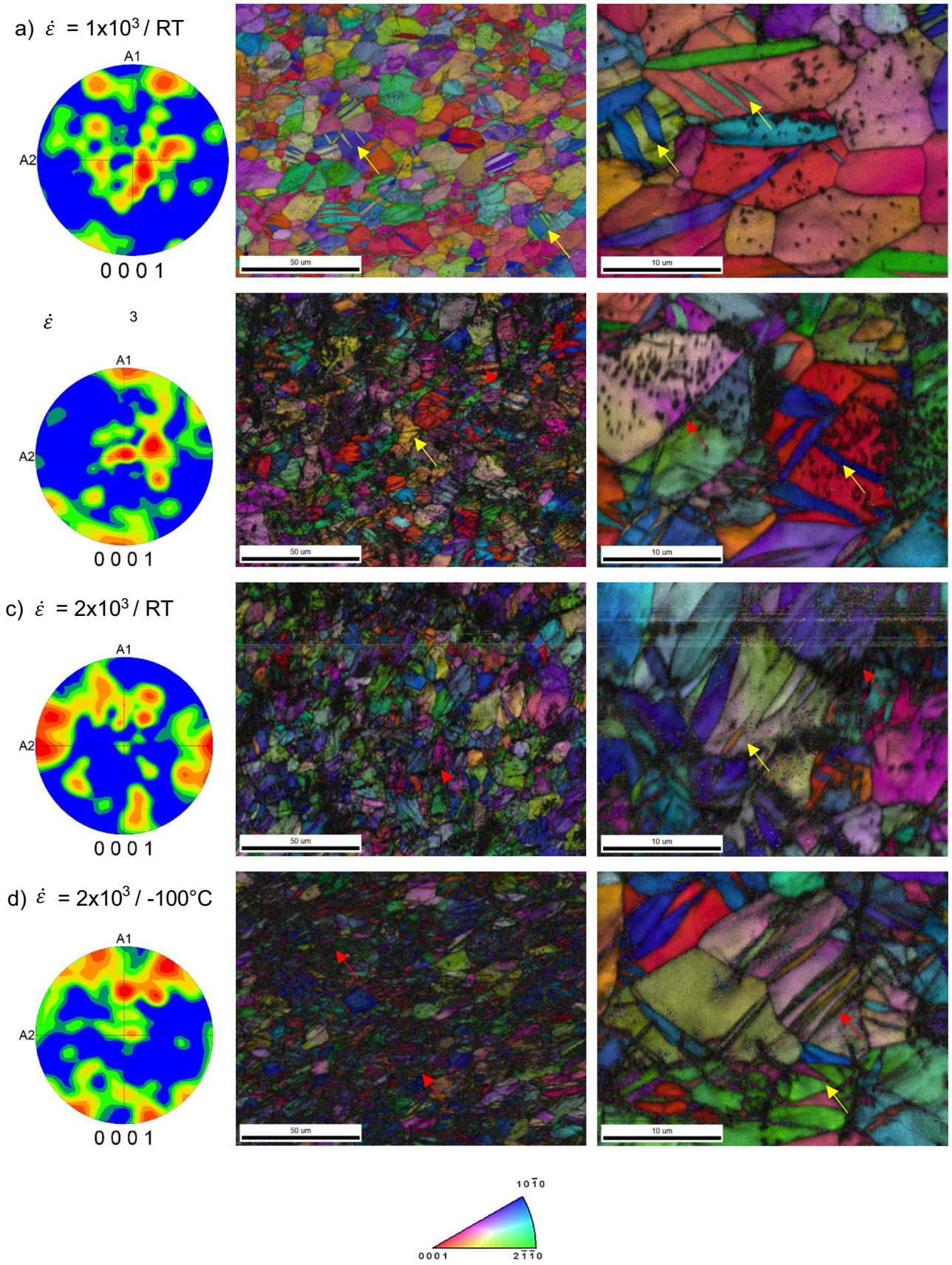

Fig. 4 IPF maps of CP-Ti deformed under various strain rate and temperature conditions: $\dot{\varepsilon} = 1 \times 10^3$ at room temperature (**a**) and at − 100 °C (**b**); $\dot{\varepsilon} = 2 \times 10^3$ at room temperature (**c**) and at − 100 °C (**d**) with marked twins (yellow arrows) and shear bands (red arrows)

development of shear bands as strain progresses [19]. These bands manifest as elongated, highly misoriented zones that truncate existing twins and cross multiple grains, indicating the onset of localized plasticity and damage evolution.

At the higher strain rate of $\dot{\varepsilon} = 2 \times 10^3\ s^{-1}$, the room temperature response (Fig. 4c) displays increased twin activity compared to the lower strain rate, with more densely packed and intersecting twins. The higher density of twinning features suggests a greater demand for strain accommodation, with twinning operating more extensively in grains oriented favorably with respect to the loading direction [17]. However, several regions exhibit fragmented grain structures and abrupt orientation changes, indicative of incipient shear localization. This implies that while twinning remains dominant at room temperature, the higher strain rate promotes the transition toward more localized deformation mechanisms. Under the most extreme condition—high strain rate and low temperature (Fig. 4d)—the IPF maps show extensive deformation twinning in conjunction with pervasive orientation fragmentation and disrupted grain structures. Twins are often intersected or terminated by bands of misoriented regions, which are consistent with shear band formation. These features suggest that twinning is rapidly activated at early stages but is ultimately insufficient to accommodate the full extent of imposed strain, especially under low-temperature conditions where dislocation slide is severely restricted. The dominance of shear bands (red arrows) under these conditions reflects the material's tendency to localize strain when both temperature and strain rate hinder homogeneous deformation mechanisms. Collectively, these observations indicate a clear interaction and competition between deformation twinning and shear banding in dynamically compressed CP-Ti, governed strongly by temperature and strain rate. Twinning is the primary mechanism at room temperature across strain rates, while at − 100 °C, despite an initial increase in twin activity, shear band formation appeared with rising strain rate. The IPF maps, thus, provide direct evidence of a temperature- and rate-dependent transition in deformation mode, with significant implications for the dynamic ductility and failure resistance of hexagonal close-packed metals.

3.3 Shear-twining competition during dynamic deformation

At room temperature, IPF maps revealed widespread activation of deformation twinning across the microstructure. The presence of twins was evident through the occurrence of sharp, elongated domains within grains, exhibiting the characteristic ~ 85° reorientation relative to the parent orientation. These twins were distributed in grains that were favorably oriented for twinning, as indicated by the change in color contrast in the IPF maps corresponding to crystallographic rotation along the loading direction. The overall grain structure remained relatively intact, and although localized orientation changes were observed near grain boundaries and within some grains, the microstructure was still dominated by twin-related features (Fig. 5a). Shear bands, while occasionally present, appeared as narrow, linear regions of intense orientation gradients often cutting across multiple grains and disrupting prior twin structures. However, their occurrence was relatively limited, suggesting that at room temperature, twinning remained the primary mode of accommodating dynamic plastic deformation.

On the other hand, the IPF maps of specimens compressed at − 100 °C showed a marked increase in twinning activity, with significantly thicker and more numerous twin lamellae observed throughout the microstructure (Fig. 5b). The contrast changes in IPF orientation colors indicated more extensive crystallographic reorientation due to twinning. However, as strain increased, regions of abrupt and severe orientation discontinuities became more prominent, appearing as sharply misoriented zones that extended across grains and twins alike. These features are characteristic of shear bands and reflect intense localized deformation that surpasses the accommodation capability of twinning alone. The IPF maps clearly showed instances where shear bands pass through twin lamellae or altered their propagation paths, indicating that at low temperature, while twinning initiates deformation, it is increasingly overtaken by shear band formation as strain progresses.

The comparative analysis of IPF maps, thus, highlights a temperature-dependent evolution of deformation mechanisms in CP-Ti under high-strain-rate loading (Fig. 5c, d). At room temperature, deformation twinning is the dominant response, effectively accommodating strain in combination with dislocation slip, while shear bands

 https://doi.org/10.1007/s43452-025-01317-0

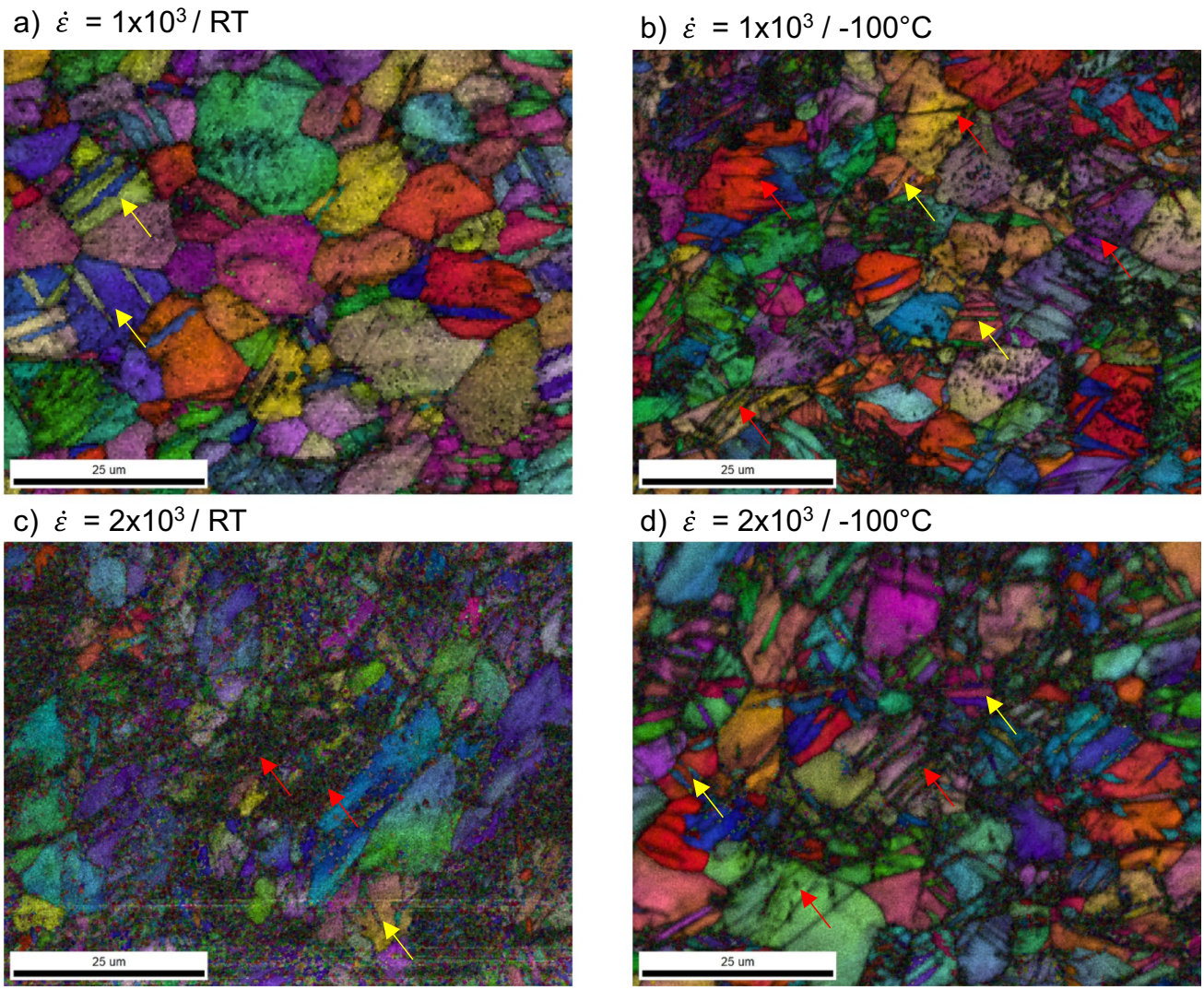

Fig. 5 IPF maps of CP-Ti deformed under various strain rate and temperature conditions: $\dot{\varepsilon} = 1 \times 10^3$ at room temperature (**a**) and at − 100 °C (**b**); $\dot{\varepsilon} = 2 \times 10^3$ at room temperature (**c**) and at − 100 °C (**d**) with marked twins (yellow arrows) and shear bands (red arrows)

appear only at more advanced stages of deformation. At − 100 °C, twinning is more extensively activated due to reduced slip activity, but the early onset of severe orientation fragmentation suggests a stronger contribution from shear localization. The IPF evidence indicates that twinning and shear bands coexist and interact, with shear bands ultimately prevailing as the dominant mechanism of plastic flow under low-temperature dynamic loading conditions.

The evolution of Low-Angle Boundaries (LABs) and High-Angle Boundaries (HABs) during dynamic deformation of CP-Ti shows a clear dependence on both strain rate and temperature, as evidenced by EBSD grain boundary analysis and quantified misorientation data (Table 1; Fig. 6). At room temperature and lower strain rates (Fig. 6a, c), deformation is primarily accommodated by dislocation slip, allowing for the formation of LABs through sub-grain development. This is reflected in the highest LAB fraction (0.252) under the 1×10^3 s^{-1} and 22 °C condition. As the strain rate increases at room temperature (Fig. 6c), LABs decrease (0.146), while HABs increase (0.830), indicating more severe orientation gradients and enhanced grain subdivision. This trend suggests that the increasing strain rate imposes greater mechanical energy, surpassing the accommodation capacity of

Table 1 Misorientation angle values for different strain rates

	$\dot{\varepsilon} = 1 \times 10^3$ 1/s			$\dot{\varepsilon} = 2 \times 10^3$ 1/s		
	2°–5°	5°–15°	15°–180°	2°–5°	5°–15°	15°–180°
Deformed at room temperature	0.252	0.027	0.721	0.146	0.024	0.830
Deformed at − 100 °C	0.173	0.029	0.798	0.124	0.030	0.846

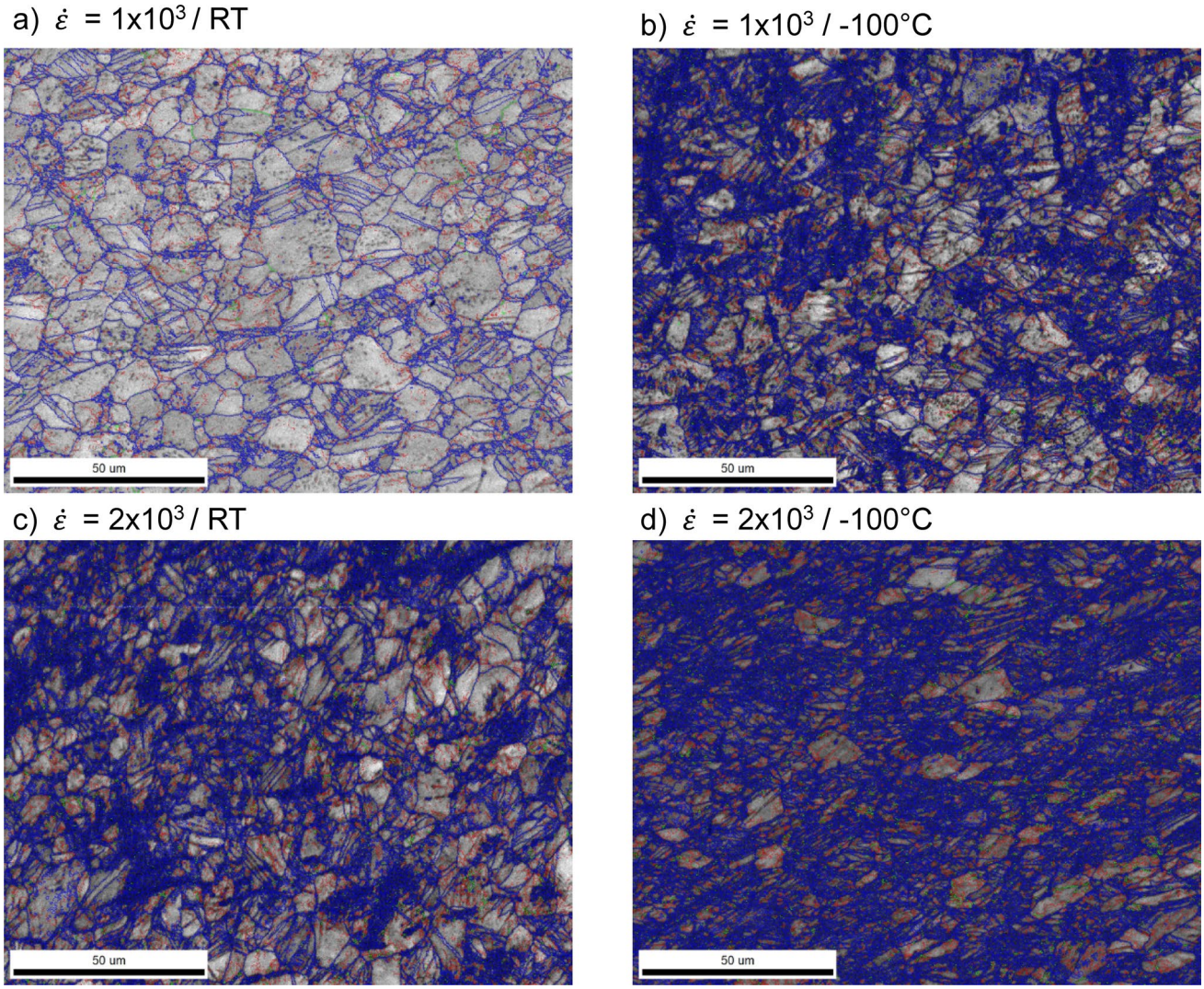

Fig. 6 Grain boundary maps of CP-Ti deformed under various strain rate and temperature conditions: $\dot{\varepsilon} = 1 \times 10^3$ at room temperature (**a**) and at − 100 °C (**b**); $\dot{\varepsilon} = 2 \times 10^3$ at room temperature (**c**) and at − 100 °C (**d**)

dislocation mechanisms and leading to elevated twinning activity and possibly incipient shear localization. Under low-temperature conditions, the LAB fraction is consistently lower than at room temperature, with the lowest value (0.124) observed at − 100 °C and 2×10^3 s^{-1} (Fig. 6b, d). This reduction reflects the restricted dislocation mobility and diminished capacity for sub-grain formation. Concurrently, HAB fractions increase with both decreasing temperature and rising strain rate, peaking at 0.846 under the most extreme conditions. This indicates a strong dominance of twinning and shear banding, which introduce abrupt orientation changes, leading to substantial

grain fragmentation and misorientation. The transition from LAB to HAB dominance under high strain rate and low temperature reflects a shift in the primary deformation mechanisms—from dislocation-mediated slip toward twinning and localized shear. This evolution aligns with EBSD IPF map observations, which show increasingly disrupted grain structures and pervasive orientation fragmentation at − 100 °C.

3.4 Mechanical–microstructure interplay

The mechanical response of CP-Ti under dynamic compression, as shown in the true stress–strain curves (Fig. 3), correlates well with the microstructural evolution observed in the EBSD IPF maps. At both strain rates, deformation at − 100 °C results in significantly higher flow stresses compared to room temperature, reflecting the increased resistance to plastic deformation at lower temperatures. This is attributed to the suppression of dislocation mobility, which in turn enhances the role of alternative deformation mechanisms such as deformation twinning and promotes earlier onset of shear localization. At the lower strain rate $\dot{\varepsilon} = 2 \times 10^3$ s^{-1}, the material deformed at room temperature shows moderate yield and flow stresses, accompanied by a relatively steady hardening response. This is consistent with the EBSD observations (Fig. 5a), which show widespread but controlled twinning activity, with limited evidence of grain fragmentation or shear banding. Twinning accommodates plastic strain effectively without inducing strong strain localization, allowing for sustained strain hardening. In contrast, the sample tested at the same strain rate but at − 100 °C (Fig. 5b) displays a higher yield stress and a more pronounced initial hardening rate, followed by a plateau or slight softening at larger strains. The corresponding IPF maps reveal a much more heterogeneous microstructure with dense twinning and signs of emerging shear bands. The elevated strength and reduced ductility under low-temperature conditions reflect the transition from homogeneous deformation by twinning to more localized strain accommodation through shear band formation, which ultimately limits strain hardening capacity.

At the higher strain rate of $\dot{\varepsilon} = 2 \times 10^3$ s^{-1}, the differences between the two temperatures become even more pronounced. At room temperature (Fig. 5c), the material exhibits increased flow stress relative to the lower strain rate, along with evidence of strain hardening, but the onset of flow softening is more abrupt. The IPF maps show intensified twinning and early stage shear localization, indicating that the elevated strain rate begins to exceed the capacity of twinning alone to accommodate strain, leading to localized deformation. Under the combined effect of high strain rate and low temperature (Fig. 5d), the material shows the highest yield stress. The EBSD maps correlate with this behavior, showing a heavily deformed microstructure dominated by both extensive twinning and pervasive shear banding. While twinning contributes significantly to strain accommodation across all conditions, its effectiveness diminishes at high strain rates and low temperatures. In these regimes, twinning becomes insufficient to homogenize deformation, and the formation of shear bands leads to premature flow softening and reduced ductility.

4 Material modeling and model calibration

Accurate modeling of material behavior necessitates the formulation of representative equations that capture the fundamental mechanisms governing deformation. In metal stamping processes, flow stress can be characterized by Hooke's law as follows:

$$\sigma = E\left(\varepsilon_{\mathrm{T}} - \varepsilon_{\mathrm{P}}\right), \tag{1}$$

where ε_{T}—total true strain, ε_p—plastic strain, and E—Young's modulus. When considering viscoplastic flow, the rate of plastic deformation is influenced by the instantaneous flow stress, the initial yield stress, and isotropic dislocation hardening. This relationship can be expressed as:

$$\dot{\varepsilon}_{\mathrm{P}} = \left(\frac{\sigma - R - k}{K}\right)^{n_1}, \tag{2}$$

where $\dot{\varepsilon}_{\mathrm{p}}$—plastic strain rate, σ—flow stress, R—stress due to dislocation hardening, k—initial yield stress, and K, n_1—material constants. Given that dynamic deformation at low temperatures does not significantly alter grain size (Fig. 8), the proposed model does not incorporate grain size evolution or softening mechanisms associated with dynamic recrystallization.

According to classical work-hardening theory [20–22], the hardening parameter in Eq. (2) is a function of the dislocation density ρ:

$$R = B\bar{\rho}^{-0.5}, \tag{3}$$

where B is a material-dependent coefficient. The evolution of dislocation density, transitioning from an initial value of zero to a saturated state, results from the interplay of dislocation accumulation due to plastic deformation and annihilation driven by recovery processes. This evolution is governed by the following equation:

$$\dot{\bar{\rho}} = A\left(1 - \bar{\rho}\right)\dot{\varepsilon_{\mathrm{P}}} - C\,\bar{\rho}, \tag{4}$$

where $\bar{\rho}$—normalized dislocation density, and A and C are the material parameters.

Under low-temperature conditions, the yield stress is influenced not only by plastic deformation caused by dislocations but also by thermally activated mechanisms. The evolution of this process can be described as:

$$\dot{k} = D\dot{\varepsilon}_{\mathrm{P}}^{n_2}, \tag{5}$$

where D—temperature-dependent diffusion parameter, n_2—material constant. It has to be emphasized that K, n_1, n_2, B, A, C, and D depend on the instantaneous temperature, which can be well expressed using the Arrhenius equation:

$$X = X_0 \exp\left(\frac{Q_X}{kT}\right), \tag{6}$$

where X_0—coefficient of the applied parameter, k—universal gas constant of 8.31 J/mol/K, T—absolute temperature and Q_X—activation energy. The temperature-dependent parameters are listed in Table 2.

The developed constitutive model, represented by Eqs. (1)–(6), provides a comprehensive description of the flow behavior of CP-Ti under low-temperature conditions. The material constants are then calibrated and optimized using a Genetic Algorithm, as outlined in the flow chart shown in Fig. 7, resulting in the predicted solid lines presented in Fig. 8 and finally shown in Table 3.

The experimental data and corresponding numerical results obtained using the developed material model are illustrated in Fig. 8, where the symbols denote the experimental measurements, and the solid lines represent the model predictions. As observed, the model demonstrates a high level of agreement (~ 5%) with the experimental data, validating its accuracy. Notably, the strain-rate sensitivity of titanium allows for the application of a classical viscoplastic model to effectively capture its deformation behavior under low-temperature conditions. Therefore, the proposed model serves as a reliable tool for predicting material behavior in finite element simulations. This predictive capability is particularly important to industrial forming processes, wherein precise control over stress

Table 2 List of temperature-dependent parameters

$n_1 = n_{10}\exp(Q_{n10}/\mathrm{kT})$	$B = B_0\exp(Q_b/kT)$	$E = E_0\exp(Q_e/kT)$
$n_2 = n_{20}\exp(Q_{n20}/\mathrm{kT})$	$C = C_0\exp(Q_c/kT)$	
$K = K_0\exp(Q_k/\mathrm{kT})$	$D = D_0\exp(Q_d/kT)$	

$k = 8.31$ J/mol/K; T is absolute temperature in K

 https://doi.org/10.1007/s43452-025-01317-0

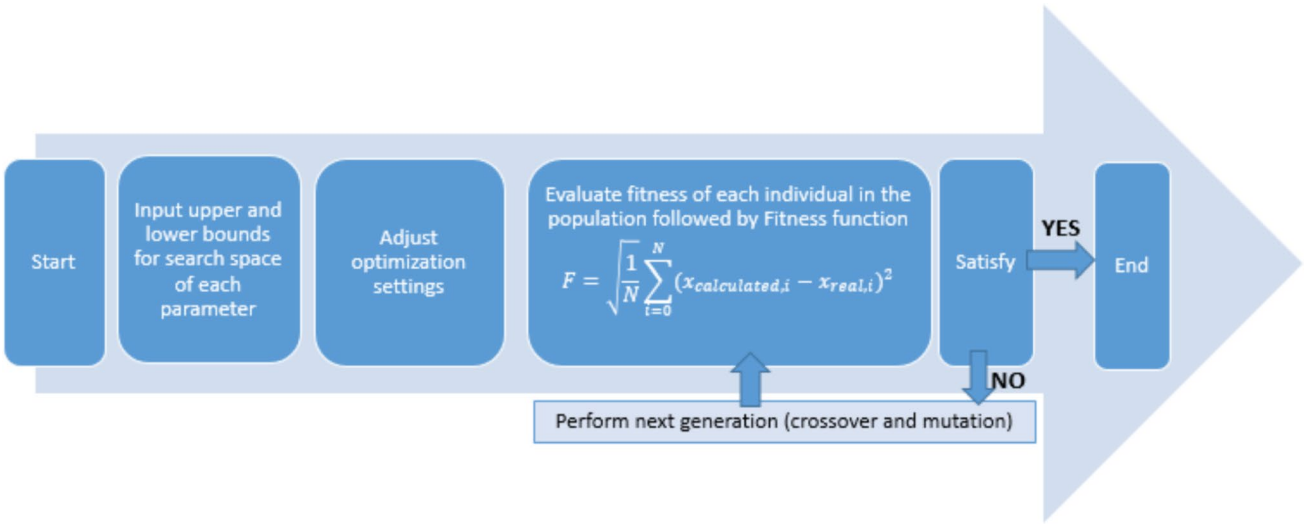

Fig. 7 The flow chart of Genetic Algorithm to calibrate and optimize the viscoplastic constitutive equations

state, material flow, strain localization, and failure initiation is paramount to ensuring process robustness and component performance [23, 24].

5 Conclusion

The main findings of this research were as follows:

- CP-Ti exhibits pronounced strengthening under dynamic compression at − 100 °C, with flow stresses increasing by up to ~ 30% compared to room temperature at equivalent strain rates. This is attributed to reduced dislocation mobility and suppressed dynamic recovery.
- At room temperature, deformation is primarily governed by dislocation slip and extensive {10–12}⟨ 10−11 ⟩ tensile twinning. Under low-temperature conditions of − 100 °C, twinning is initially intensified but is progressively supplanted by the formation of shear bands as strain increases and strain rate rises.
- EBSD analysis demonstrated that while room temperature deformation preserves equiaxed grain morphology with uniform twinning, low-temperature deformation leads to significant orientation fragmentation and shear localization.
- The mechanism-based viscoplastic constitutive model successfully reproduced the experimental stress–strain response across all conditions. Calibration using a strain-rate-sensitive, thermally activated formulation enabled accurate prediction with < 5% error, validating its use for finite element simulations in low-temperature forming applications.
- The observed enhancement in strength and alteration of deformation mechanisms at − 100 °C support the potential for low-temperature, high-rate forming of titanium components, such as in the Fast Alloy Stamping Technology (FAST) framework, providing improved mechanical performance without compromising microstructural integrity.

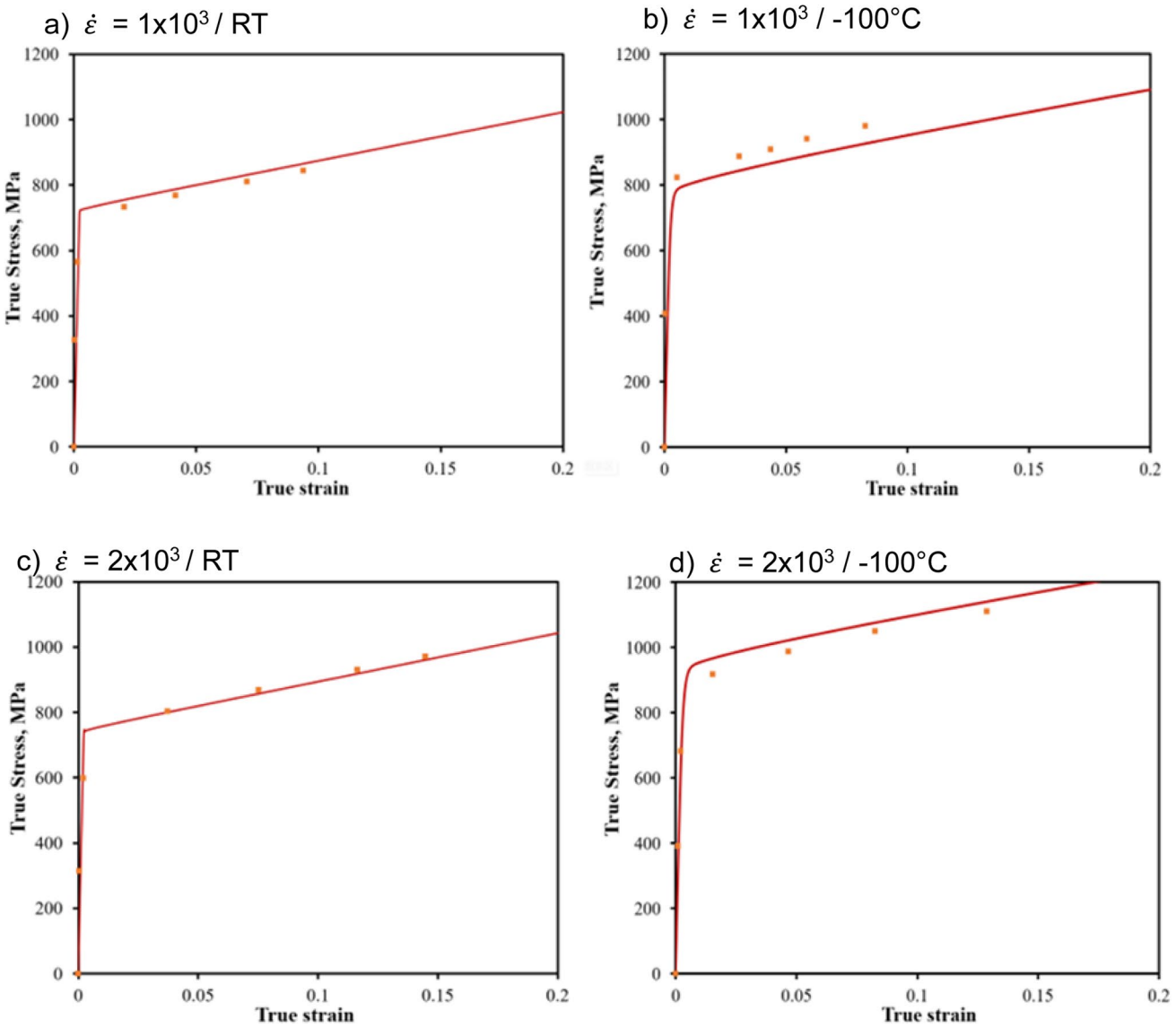

Fig. 8 Comparison of the stress–strain curves obtained from the experiments (points) and numerical (line) calculations at room and low temperature: $\dot{\varepsilon} = 1\times10^3$ at room temperature (**a**) and at − 100 °C (**b**); $\dot{\varepsilon} = 2\times10^3$ at room temperature (**c**) and at − 100 °C (**d**)

Table 3 Material parameters of the model

Constant	E_0	Q_E	K_0	Q_K	A_0	Q_A	B_0	Q_B
Value	36,221	− 249.3	492.75	− 5401.5	300.8	− 4384.9	0.48	6648
Unit	MPa	J/mol	MPa	J/mol	–	J/mol	MPa	J/mol
Constant	C_0	Q_C	D_0	Q_D	n_{10}	Q_{n10}	n_{20}	Q_{n20}
Value	0.272	3192.1	897.8	1246.5	22.19	− 3549	1.1	− 237.5
Unit	–	J/mol	MPa	J/mol	–	J/mol	–	J/mol

Acknowledgements The author would like to express his gratitude to Patryk Modrzejewski for his kind help during the experimental part of this work.

Funding This work was co-financed by the Military University of Technology under research project UGB No. 531-000048-W200-22.

Data availability The data will be available on reasonable request.

Declarations

Conflict of interest The authors declare that they have no known competing financial interests or personal relationships that could have appeared to influence the work reported in this paper.

Ethical approval This article does not contain any studies with human participants or animals performed by any of the authors.

References

1. Xu Y, Aceves Lopez M, Zhou J, Farbaniec L, Patsias S, Macdougall D, et al. Experimental analysis of the multiaxial failure stress locus of commercially pure titanium at low and high rates of strain. Int J Impact Eng. 2022;170:104341. https://doi.org/10.1016/j.ijimpeng.2022.104341.
2. Wei Y, Zhang C, Yuan Y, Chen P, Huang C, Li J, et al. Blast response of additive manufactured Ti–6Al–4V sandwich panels. Int J Impact Eng. 2023;176:104553. https://doi.org/10.1016/j.ijimpeng.2023.104553.
3. Kopec M, Wang K, Politis DJ, Wang Y, Wang L, Lin J. Formability and microstructure evolution mechanisms of Ti6Al4V alloy during a novel hot stamping process. Mater Sci Eng A. 2018;719:72–81. https://doi.org/10.1016/j.msea.2018.02.038.
4. Bao Q, Zhao C, Wang K, Zhao J, Cui S, Gao B, et al. A novel integrated hot forming with in-situ stress relaxation-aging for titanium alloy thin-walled components. J Manuf Process. 2024;131:1296–308. https://doi.org/10.1016/j.jmapro.2024.09.113.
5. Wang K, Kopec M, Chang S, Qu B, Liu J, Politis DJ, et al. Enhanced formability and forming efficiency for two-phase titanium alloys by fast light alloys stamping technology (FAST). Mater Des. 2020;108948:1–25. https://doi.org/10.1016/j.matdes.2020.108948.
6. Wang K, Wang L, Zheng K, He Z, Politis DJ, Liu G, et al. High-efficiency forming processes for complex thin-walled titanium alloys components: state-of-the-art and perspectives. Int J Extrem Manuf. 2020;2:032001. https://doi.org/10.1088/2631-7990/ab949b.
7. Lei L, Zhu Q, Zhao Q, Yang M, Yang W, Zeng W, et al. Low-temperature impact toughness and deformation mechanism of CT20 titanium alloy. Mater Charact. 2023;195:112504. https://doi.org/10.1016/j.matchar.2022.112504.
8. Li D, Meng ZC, Shen YY, Zhang JH, Hu M, Qiu JK, et al. Study of low-temperature impact deformation behavior of Ti–6Al–4V alloy. Vacuum. 2024;222:113066. https://doi.org/10.1016/j.vacuum.2024.113066.
9. Kopec M, Liu X, Gorniewicz D, Modrzejewski P, Zasada D, Jóźwiak S, et al. Mechanical response of 6061–T6 aluminium alloy subjected to dynamic testing at low temperature: experiment and modelling. Int J Impact Eng. 2024;185:104843. https://doi.org/10.1016/j.ijimpeng.2023.104843.
10. Lin H, Jin G, Zhan Q, et al. Mechanical properties and constitutive model of TC4 titanium alloy at cryogenic. J Mater Eng Perform. 2024;33:13731–43. https://doi.org/10.1007/s11665-023-08955-6.
11. Chong Y, Gholizadeh R, Tsuru T, et al. Grain refinement in titanium prevents low temperature oxygen embrittlement. Nat Commun. 2023;14:404. https://doi.org/10.1038/s41467-023-36030-0.
12. Jeon B, Lee MS, Jun TS, Jeong Y. Temperature-dependent behavior of CP-Ti interpreted via self-consistent crystal plasticity simulation. Mater Sci Eng A. 2024;890:145904. https://doi.org/10.1016/j.msea.2023.145904.

13. Lee MS, Jo AR, Hwang SK, Hyun YT, Jun TS. The role of strain rate and texture in the deformation of commercially pure titanium at cryogenic temperature. Mater Sci Eng A. 2021;827:142042. https://doi.org/10.1016/j.msea.2021.142042.
14. Liu D, Yang D, Hou Y, Li Y, Wang G, Yi H. Strain rate effects on mechanical properties, microstructural evolution, and deformation mechanisms of high manganese steels. J Mater Sci Technol. 2025;237:219–55. https://doi.org/10.1016/j.jmst.2025.03.026.
15. Yang H, Li H, Sun H, Zhang YH, Liu X, Zhan M, et al. Anisotropic plasticity and fracture of alpha titanium sheets from cryogenic to warm temperatures. Int J Plast. 2022;156:103348. https://doi.org/10.1016/j.ijplas.2022.103348.
16. Chen C, Han D, Song Y, Wang M, Li Y, Xu S. Thermal stability of deformation twins in cryogenic rolled CP-Ti. Mater Charact. 2023;196:112587. https://doi.org/10.1016/j.matchar.2022.112587.
17. Tsukamoto G, Kunieda T, Mitsuhara M, Nakashima H. Effect of twinning deformation on work hardening in commercially pure titanium. Mater Sci Eng A. 2022;840:142907. https://doi.org/10.1016/j.msea.2022.142907.
18. Guo Y, Ruan Q, Zhu S, Wei Q, Lu J, Hu B, et al. Dynamic failure of titanium: temperature rise and adiabatic shear band formation. J Mech Phys Solids. 2020;135:103811. https://doi.org/10.1016/j.jmps.2019.103811.
19. Chakraborty A, Roy S. Shear localization and shear banding: a review about the complex interplay between material, microstructural and process variables. Mater Charact. 2024;218:114501. https://doi.org/10.1016/j.matchar.2024.114501.
20. Garrett RP, Lin J, Dean TA. An investigation of the effects of solution heat treatment on mechanical properties for AA 6xxx alloys: experimentation and modelling. Int J Plast. 2005;21:1640–57. https://doi.org/10.1016/j.ijplas.2004.11.002.
21. Schneider R, Grant RJ, Sotirov N, Falkinger G, Grabner F, Reichl C, et al. Constitutive flow curve approximation of commercial aluminium alloys at low temperatures. Mater Des. 2015;88:659–66. https://doi.org/10.1016/j.matdes.2015.09.034.
22. Lee W-S, Lin C-R. Deformation behavior and microstructural evolution of 7075–T6 aluminum alloy at cryogenic temperatures. Cryogenics. 2016;79:26–34. https://doi.org/10.1016/j.cryogenics.2016.07.007.
23. Wang D, Xu Z, Han Y, Su M, Huang F. Coupled effect of stress state and strain rate on ductile fracture of Ti6Al4V alloy. Int J Impact Eng. 2024;187:104898. https://doi.org/10.1016/j.ijimpeng.2024.104898.
24. Zhou T, Wu J, Che J, Wang Y, Wang X. Dynamic shear characteristics of titanium alloy Ti–6Al–4V at large strain rates by the split Hopkinson pressure bar test. Int J Impact Eng. 2017;109:167–77. https://doi.org/10.1016/j.ijimpeng.2017.06.007.

Authors and Affiliations

Mateusz Kopec[1,3] · Magdalena Łazińska[2] · Jacek Janiszewski[2]

✉ Mateusz Kopec
mkopec@ippt.pan.pl

[1] Institute of Fundamental Technological Research Polish Academy of Sciences, 5b Pawinskiego Str., 02-106 Warsaw, Poland

[2] Military University of Technology, 00-908 Warsaw, Poland

[3] College of Science and Engineering, University of Derby, Derby, UK, Markeaton Street, DE22 3AW